HEALTH AND MEDICINE

PDLLA-Zn-nitrided Fe bioresorbable scaffold with 53-μm-thick metallic struts and tunable multistage biodegradation function

Danni Shen[1†], Haiping Qi[2†], Wenjiao Lin[2†], Wanqian Zhang[2,3], Dong Bian[1,2], Xiaoli Shi[2], Li Qin[2], Gui Zhang[2], Wenchao Fu[2], Kefei Dou[4], Bo Xu[4], Zhenyuan Yin[5], Jiancun Rao[6], Mazeni Alwi[7], Shuhan Wang[8], Yufeng Zheng[1,5]*, Deyuan Zhang[2]*, Runlin Gao[4]*

Balancing the biodegradability and mechanical integrity of a bioresorbable scaffold (BRS) with time after implantation to match the remodeling of the scaffolded blood vessel is important, but a key challenge in doing so remains. This study presents a novel intercalated structure of a metallic BRS by introducing a nanoscale Zn sacrificial layer between the nitrided Fe platform and the sirolimus-carrying poly(D,L-lactide) drug coating. The PDLLA-Zn-FeN BRS shows a multistage biodegradation behavior, maintaining mechanical integrity at the initial stage and exhibiting accelerated biodegradation at the subsequent stage in both rabbit abdominal aortas and human coronary arteries, where complete biodegradation was observed about 2 years after implantation. The presence of the nanoscale Zn sacrificial layer with an adjustable thickness also contributes to the tunable biodegradation of BRS and allows the reduction of the metallic strut thickness to 53 μm, with radial strength as strong as that of the current permanent drug-eluting stents.

INTRODUCTION

The landscape of coronary angioplasty has changed markedly over the last decades from the plain old balloon angioplasty to the development and use of bare metal stents and drug-eluting stents (DESs) and then of bioresorbable scaffolds (BRSs) (*1*). BRS has drawn much interest because of its superiority over DES, as the permanent presence of DES causes inflammation and hyperplasia in the scaffolded region, leading to long-term side effects. In addition, there is increasing evidence that permanent caging by stents will bring about late vascular consequences, such as stent thrombosis (*2*, *3*) and chronic inflammation (*4*, *5*).

The development of BRS benefits from the innovation of scaffold materials, from inert stainless steels and Co-Cr alloys to biodegradable polymeric and metallic materials. As regard polymeric BRS, which makes use of the polylactic acid scaffold technology, the Absorb Bioresorbable Vascular Scaffold (Absorb BVS, Abbott Vascular) was the first U.S. Food and Drug Administration–approved fully bioresorbable vascular scaffold (*6*). Although the large and randomized clinical trials of Absorb BVS seemed to show promising results with 1-year follow-up, the longer-term clinical trial results exposed certain issues, particularly its higher rate of stent thrombosis and target lesion failure than the current-generation DESs (*4*, *7*–*10*). The underlying mechanism of these issues may be related to thick struts (150 μm), strut malapposition, and uncovered struts without neointima (*6*, *9*). Absorb BVS was thus withdrawn from the market in 2017 (*6*). As for metallic BRS, magnesium-based BRS has experienced an iteration from bare absorbable metal stents (AMSs; Biotronik AG, Buelach, Switzerland) to the first- and second-generation drug-eluting absorbable metal scaffold (DREAMS and DREAMS 2G, marked as Magmaris, Biotronik AG, Buelach, Switzerland), overcoming AMS's disadvantage of extremely rapid scaffold biodegradation (*5*, *11*–*13*). Up to 25 September 2019, the clinical data of 1075 patients for Magmaris at 12-month follow-up were available in BIOSOLVE-IV (*14*). These data showed that complete bioresorption had not been achieved 1 year after implantation, and the long-term safety of the scaffold has yet to be determined. As pointed out by Jinnouchi *et al.* (*6*), the strut thickness of Magmaris is similar to that of Absorb BVS, which suggests that a long duration of dual antiplatelet therapy should be considered when using Magmaris. A direct comparison of Magmaris (strut thickness, ~150 μm) with the current-generation DES (strut thickness, 60 to 80 μm) from the same company (Orsiro, Biotronik AG, Buelach, Switzerland) also demonstrated higher late lumen loss and restenosis rate in Magmaris (*15*).

In 2001, Peuster *et al.* (*16*) proved the preliminary feasibility of the pure Fe BRS. However, its slow biodegradation rate, as revealed by the fact that large portions of the struts remained intact in the porcine descending aorta 1 year after implantation, remains a major obstacle to its clinical application (*17*). We thus designed a nitrided Fe BRS, with the U.S. patent issued in 2017 (*18*). The nitriding process enhanced the radial strength of the scaffold to 171 kPa from the bare Fe BRS's 92 kPa, allowing a thinner strut design. We thus made the strut thickness of the nitrided Fe BRS much lower (70 μm) than those of Absorb BVS and Magmaris (150 μm). Although the nitrided Fe BRS showed faster biodegradation than the bare Fe BRS, only ~76% of it had degraded in the rabbit abdominal aorta 36 months after implantation (*19*). To further shorten the

[1]Beijing Advanced Innovation Center for Materials Genome Engineering and School of Materials Science and Engineering, Peking University, Beijing 100871, China. [2]National and Local Joint Engineering Laboratory of Interventional Medical Biotechnology and System, Lifetech Scientific (Shenzhen) Co. Ltd., Shenzhen 518110, China. [3]State Key Laboratory of Molecular Engineering of Polymers, Department of Macromolecular Science, Fudan University, Shanghai 200433, China. [4]Department of Cardiology, Fuwai Hospital, Chinese Academy of Medical Sciences and Peking Union Medical College, Beijing 100037, China. [5]BioMed-X Center, Academy for Advanced Interdisciplinary Studies, Peking University, Beijing 100871, China. [6]AIM Lab, Maryland NanoCenter, University of Maryland, College Park, MD 20742, USA. [7]Paediatric Cardiology, Institut Jantung Negara (National Heart Institute), 145, Jalan Tun Razak, Kuala Lumpur 50400, Malaysia. [8]Shen Zhen Testing Center of Medical Devices, Shenzhen 518057, China.
*Corresponding author. Email: yfzheng@pku.edu.cn (Y.Z.); zhangdeyuan@lifetechmed.com (D.Z.); gaorunlin@citmd.com (R.G.)
†These authors contributed equally to this work.

biodegradation period of the scaffold and to balance its biodegradability and mechanical integrity, we designed a poly(D,L-lactide) (PDLLA)–Zn-nitrided Fe BRS by intercalating a nanoscale Zn sacrificial layer between the nitrided Fe platform and the PDLLA drug coating, and it has been preliminarily proven to be feasible (*20*, *21*). Here, we report a long-term (24-month) systematic investigation of the in vivo degradation behavior of PDLLA-Zn-nitrided Fe BRS in the rabbit abdominal aorta and the preliminary results of the first in-human implantation obtained 26 months after implantation. We reduced the thickness of the PDLLA-Zn-nitrided Fe BRS's metallic strut to ~53 μm, making it currently the thinnest strut used in clinical trials and applications of BRS and permanent DES to the best of our knowledge.

RESULTS

Microstructure characterization

As shown in Fig. 1A, the entire strut of the PDLLA-Zn-nitrided Fe BRS consists of three layers: a PDLLA drug coating (blue), a nanoscale Zn sacrificial layer (red), and a nitrided Fe platform (gray). The cross-sectional morphology is also revealed by its scanning electron microscopy (SEM) images (Fig. 1, B and C). The nitrided Fe platform and Zn sacrificial layer are 52.80 ± 0.13 μm and 811 ± 40 nm thick, respectively. We coated the substrate with PDLLA drug coating, with a 12.58 ± 0.34 μm average abluminal thickness and a 9.23 ± 0.30 μm average luminal thickness. We directly obtained the x-ray photoelectron spectroscopy (XPS) and x-ray diffraction (XRD) patterns of the experimental samples after the electroplating of the nanoscale Zn sacrificial layer (Fig. 1, D and E), and they indicated the successful deposition of the crystalline zinc nanofilm on the nitrided Fe platform. The peak of Zn LMM at 494.8 eV in the XPS spectrum suggests that the nanoscale Zn sacrificial layer was in its elemental state. The XRD analysis revealed that the peaks were due to the zinc and the nitrided Fe matrix. The characteristic peaks at 2θ = 36.2°, 38.8°, 43.1°, 54.2°, and 70.0° in the diffraction pattern corresponded to the (002), (100), (101), (102), and (103) planes of the Zn phase (no. 00-004-0831). The peaks at 2θ = 44.6°, 65.0°, and 82.3° indicated the (110), (200), and (211) planes of the nitrided Fe platform (no. 01-087-0722). Figure 1F also shows the Fourier transform infrared spectroscopy (FTIR) spectrum of the PDLLA samples, in which we detected the typical peaks of —CH_3, C—O—C, and C═O from PDLLA.

In vivo degradation behavior

PDLLA-Zn-nitrided Fe BRSs were placed in the abdominal aortas of adult New Zealand white rabbits and were kept there for 24 months for the systematic investigation of their complete in vivo degradation behavior. The biodegradation process of the PDLLA-Zn-nitrided Fe BRS after implantation is intuitively revealed by two-dimensional (2D) images of micro–computed tomography (CT)–reconstructed scaffolds, optical images, and hematoxylin and eosin (H&E) staining images (Fig. 2). Within the first 2 months after implantation, all the scaffold struts showed sharp contours in the reconstructed images (Fig. 2A), and their optical images did not show any brown biodegradation products (Fig. 2, B and C), indicating that the nitrided Fe platform remained intact at an early stage. By the end of 3 months, although the optical image showed slight

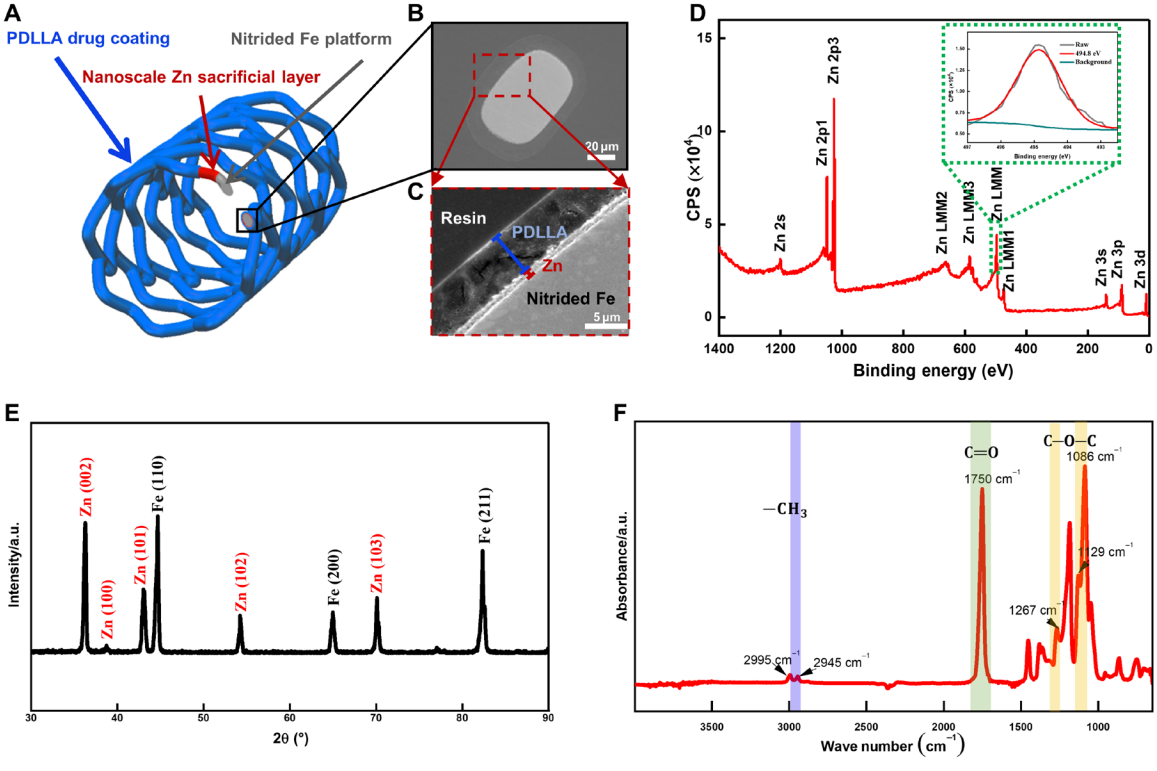

Fig. 1. Microstructure characterization of the PDLLA-Zn-nitrided Fe BRS. (**A**) Sketch map of the PDLLA-Zn-nitrided Fe BRS with a nanoscale Zn sacrificial layer intercalated between the sirolimus-eluting PDLLA coating and the nitrided Fe platform. (**B** and **C**) SEM images of the strut cross section. (**D**) XPS spectrum and (**E**) XRD pattern of the sample after nanoscale Zn sacrificial layer deposition. (**F**) FTIR spectrum of the PDLLA coating. a.u., arbitrary unit.

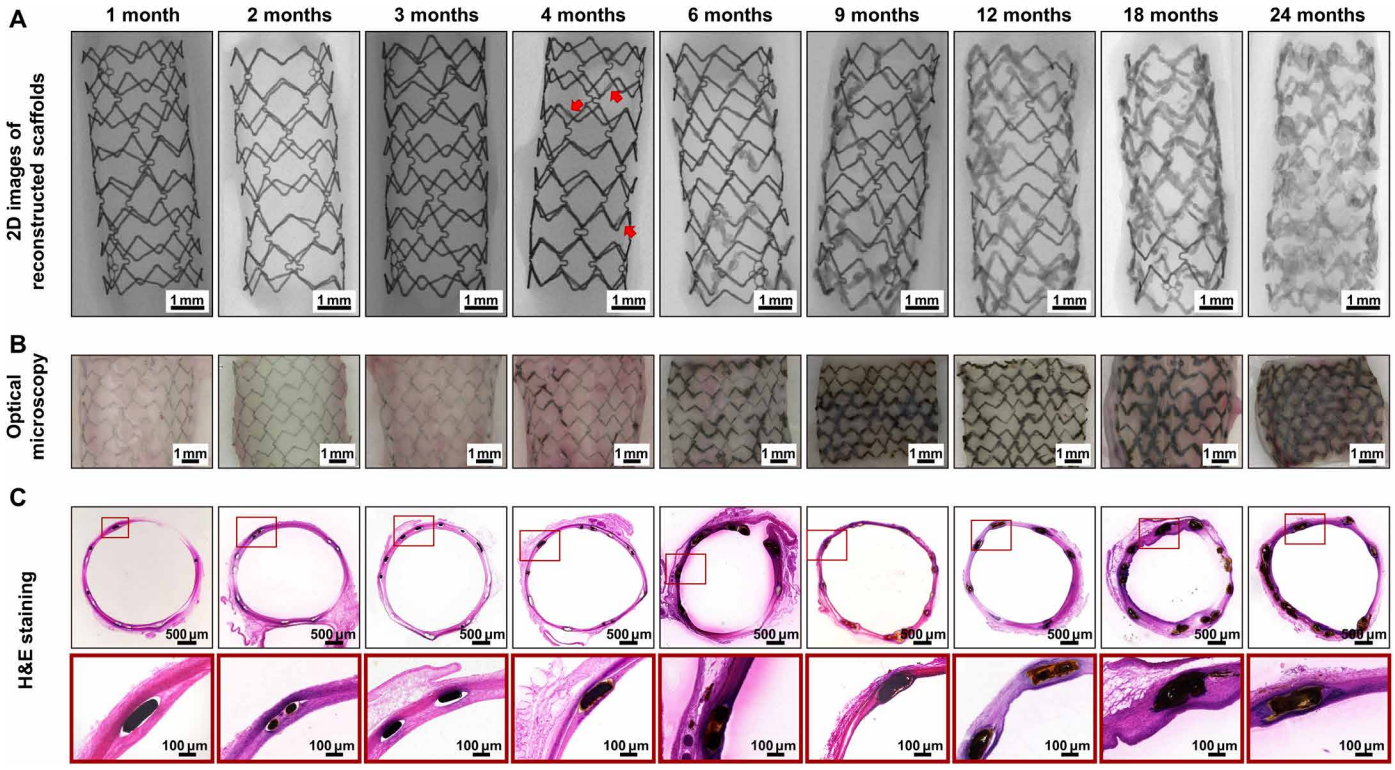

Fig. 2. In vivo degradation behavior of the PDLLA-Zn-nitrided Fe BRS in rabbit abdominal aortas at different time points after implantation. (**A**) 2D images of micro-CT reconstruction (the red arrows indicate the blurred contour areas at 4 months). (**B**) Optical micrographs of the scaffolds with vascular tissues. (**C**) Representative H&E staining images of the scaffolded vessels with high-resolution strut regions.

brown dots (biodegradation products) (Fig. 2B), the micro-CT images did not show any obvious signs of biodegradation, suggesting the extremely slight biodegradation of the nitrided Fe platform 3 months after the implantation of the BRS. The contours of the PDLLA-Zn-nitrided Fe BRS became blurred (indicated by the red arrows, Fig. 2A) and brown biodegradation products occurred 4 months postimplantation (Fig. 2, B and C). As the biodegradation process continued, more areas of the struts gradually underwent biodegradation. By the 24th month after implantation, all the scaffold struts had exhibited blurry contours, suggesting the complete biodegradation of the nitrided Fe platform, as verified by SEM and energy-dispersive spectroscopy (EDS). The biodegradation products of the PDLLA-Zn-nitrided Fe BRS, however, were not completely resorbed by the surrounding tissue.

Characterization of biodegradation products

To better understand the biodegradation process, we comprehensively evaluated the composition and distribution of the biodegradation products of the PDLLA-Zn-nitrided Fe BRS via SEM, EDS, and transmission electron microscopy (TEM) (Fig. 3). Figure 3A shows the cross-sectional SEM images of the struts of the PDLLA-Zn-nitrided Fe BRS at different time points postimplantation. The nanoscale Zn sacrificial layer could be clearly seen within the first 3 months after implantation. The signals of the Zn, O, and P elements were concentrated at the edge of the nitrided Fe platform, suggesting that a mixed layer of Zn and the zinc biodegradation product was covering the nitrided Fe platform. The sacrificial Zn layer was gradually degraded, and by the sixth month after the BRS implantation, it had been completely resorbed by the surrounding tissue (Fig. 3A and fig. S1). As for the nitrided Fe platform, within the first 3 months, the signal of the Fe element was concentrated, indicating that the biodegradation of the nitrided Fe platform had not begun or was barely perceptible, as can be seen in the micro-CT reconstruction results shown in Fig. 2A. At the fourth month postimplantation, the signal of the Fe element was split into two zones: the internal concentrated red zone and the surrounding light-red zone, representing the residual nitrided Fe platform and the biodegradation products from the nitrided Fe platform, which infiltrated the surrounding tissue. Large amounts of O and P were distributed around the nitrided Fe platform, overlapping with the area of the surrounding tissue, suggesting that the biodegradation products of the nitrided Fe platform might have been composed of Fe, O, and/or P. With prolonged time postimplantation, the PDLLA-Zn-nitrided Fe BRS was gradually degraded, and the nitrided Fe platform was completely degraded 24 months postimplantation, but some of its biodegradation products remained at the implantation site. Besides, we found that some P and Ca had been distributed at the boundary of the surrounding tissue, encapsulating the biodegradation products of the nitrided Fe platform 18 months after implantation. This indicates that the biodegradation of the nitrided Fe platform might have been accompanied by the deposition of Ca/P atop the biodegradation product layer of the nitrided Fe platform.

To obtain an in-depth understanding of the elemental distribution and biodegradation product composition during the in vivo degradation of the PDLLA-Zn-nitrided Fe BRS, we observed the sliced scaffold 3 and 24 months after implantation, via TEM. As shown in

Fig. 3B, we conducted elemental mapping in a representative region of the strut's cross section (including the nitrided Fe platform and the nanoscale Zn sacrificial layer) 3 months postimplantation. The Fe signal was concentrated, without O overlapping, while the Zn signal was dispersive, with an overlapped O signal. This indicates that the nitrided Fe platform was well protected by both the residual Zn sacrificial layer and the newly formed degradation products of the Zn sacrificial layer within the first 3 months postimplantation. We identified three regions according to their distance from the nitrided Fe platform on the basis of the selected area electron diffraction (SAED) patterns (Fig. 3C). We identified region i at the interface of the nitrided Fe platform and the Zn sacrificial layer as being in the body-centered cubic α-Fe phase, indicating an undegraded nitrided Fe platform. Regions ii and iii represent two typical biodegradation products of the nanoscale Zn sacrificial layer, and we identified them as being in the ZnO and $Zn_3(PO_4)_2$ phases, respectively (Fig. 3C). After the consumption of the Zn sacrificial layer, the nitrided Fe platform was gradually degraded in vivo. We also investigated the biodegradation products of the nitrided Fe platform 24 months after BRS implantation via TEM, as shown in Fig. 3D. The Fe and O signals were completely overlapping each other, indicating 100% biodegradation of the nitrided Fe platform. We further studied two representative regions marked as regions iv and v in Fig. 3E. In region iv, the SAED patterns demonstrated the presence of both the Fe_2O_3 and Fe_3O_4 phases, whereas the SAED pattern in region v was indexed as $Fe_3(PO_4)_2$ phase only. These results indicate that the biodegradation products of the nitrided Fe platform consisted of iron oxides in the center of the strut and iron phosphate at the superficial layer of the strut. Apart from the biodegradation products of the nitrided Fe platform directly adjacent to the strut, we found FeOOH in the vascular tissues surrounding the PDLLA coating 12 months postimplantation, which we assumed to have resulted from the redeposition of the diffused Fe^{2+} ions by the local biological chemical reaction (fig. S2).

Mass loss of different parts of the PDLLA-Zn-nitrided Fe BRS

The PDLLA-Zn-nitrided Fe BRS consists of three parts: a PDLLA drug coating, a nanoscale Zn sacrificial layer, and a nitrided Fe platform. To better understand the biodegradation process of the PDLLA-Zn-nitrided Fe BRS, we measured the weight loss of each part separately at different time points postimplantation (Fig. 4A). The PDLLA drug coating, shown in the middle of Fig. 4A, was completely degraded 18 months postimplantation. The nanoscale Zn sacrificial layer, which exhibits the steepest slope in Fig. 4A, started to react with the body fluid from the beginning and had completely turned into biodegradation products of zinc around 3 months after BRS implantation. The nitrided Fe platform, demonstrating the slowest rate in Fig. 4A, remained intact within the first 2 months but exhibited slight biodegradation at the Zn sacrificial layer/nitrided Fe interface at the time point of 3 months after BRS implantation. Then, it went through a relatively rapid biodegradation stage and a subsequent ending stage with a decreased biodegradation rate. We found the nitrided Fe platform completely degraded at the time point of 24 months (8 of the 11 scaffolds had reached 100% biodegradation then). The combined biodegradation profile of the PDLLA-Zn-nitrided Fe BRS is shown in fig. S3. The biodegradation behavior of the nitrided Fe platform can be artificially programmed through the thickness design of the nanoscale Zn sacrificial layer (fig. S4 and table S1), besides the PDLLA drug coating.

Mechanical support and its degeneration with time after BRS implantation

As shown in Fig. 4B, we measured the radial strength of the PDLLA-Zn-nitrided Fe BRS and its degeneration with time point after BRS implantation (gray line). The initial radial strength reached 131 kPa, and the scaffold provided sufficient mechanical support within the first 4 months after BRS implantation. The radial strength of the PDLLA-Zn-nitrided Fe BRS seems to have decreased rapidly, at the sixth month postimplantation, relieving the target vessel from caging after healing. In contrast, the previously reported radial strength evolution of both the pure Fe BRS (Fig. 4B, orange line) and the nitrided Fe BRS (Fig. 4B, purple line) (*19*) showed more gradual slopes, potentially preventing the restoration of the natural vasomotor function. Sufficient mechanical support and low strut thickness are usually contradictory unities of BRSs. Sufficient mechanical support prevents acute recoil and strut rupture, resulting in better efficacy. Thinner struts afford not only greater deliverability but also reduced stent-induced arterial injury and inflammation. Moreover, thinner struts facilitate endothelialization and cause less blood flow turbulence and thus decreased thrombogenicity (*22*–*24*). However, there is a trade-off between these two contradictory unities, and the previously reported BRSs have to maintain thick struts (larger than 100 μm) to reach adequate mechanical support during the biodegradation process. The PDLLA-Zn-nitrided Fe BRS showed great superiority over all the other BRSs as it demonstrated both sufficient mechanical support and low strut thickness (Fig. 4C). The excellent mechanical strength of the nitrided Fe platform makes it possible to fabricate a PDLLA-Zn-nitrided Fe BRS with much thinner struts. Besides, the intercalation of the nanoscale Zn sacrificial layer, which prevents biodegradation of the nitrided Fe platform within the first several months after BRS implantation, makes it possible to further decrease the strut thickness and prevent the loss of mechanical support stemming from the nitrided Fe platform in the first several months after implantation. It is of note that the biodegradation of the nitrided Fe platform can be held off by adjusting the thickness of the nanoscale Zn sacrificial layer.

First in-human implantation and 26-month follow-up

Figure 5 shows the results of the first in-human implantation of the PDLLA-Zn-nitrided Fe BRS. The patient had high-grade stenosis with an 80% stenosis rate in the distal right coronary artery before the procedure (Fig. 5A). We implanted a 3.5 × 18 mm PDLLA-Zn-nitrided Fe BRS in the coronary artery of the patient, and the corresponding angiographic outcome showed the open arterial lumen after implantation. We also performed serial observation through optical coherence tomography (OCT) preimplantation (after predilation), postimplantation, and at 6- and 26-month follow-up (Fig. 5B). As can be seen in Fig. 5B, the struts of the PDLLA-Zn-nitrided Fe BRS, appearing as sharply delineated bright structures with a shadow behind them under OCT, were well expanded and apposed after implantation. At 6-month follow-up, all the struts were well embedded into the intima, with no apparent recoil and no incomplete strut apposition observed (Fig. 5B). It also showed uniform, thin neointimal coverage (0.10 ± 0.05 mm), suggesting that no intimal hyperplasia occurred. Most of the struts were hardly discernible or had become arched highlighted areas with a shadow behind them (white arrow) under OCT at 26-month follow-up, suggesting that much of the scaffold had been degraded 26 months postimplantation. The arched highlighted area with a shadow behind it (white

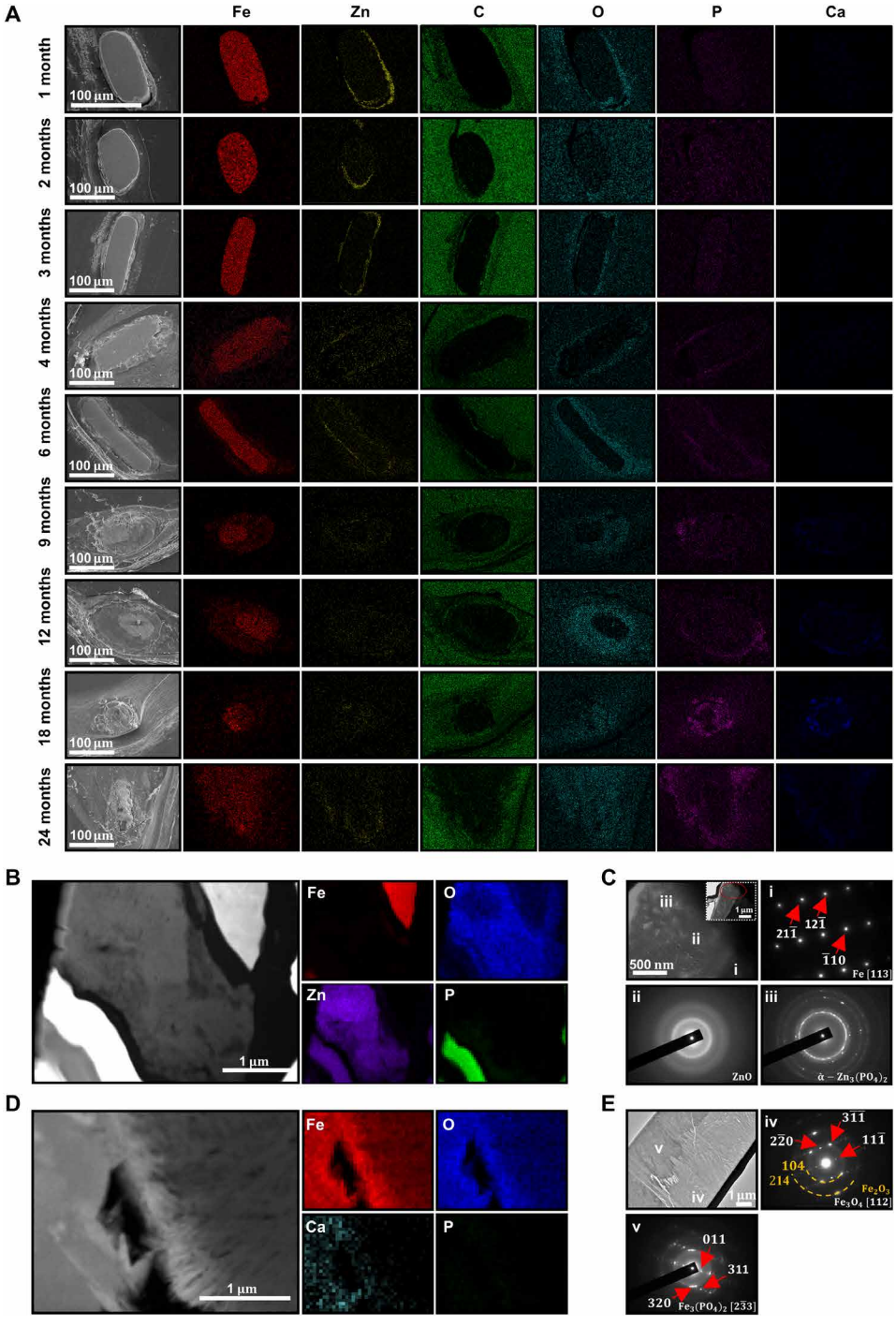

Fig. 3. Characterization of the biodegradation products of the PDLLA-Zn-nitrided Fe BRS after implantation in rabbit abdominal aortas. (**A**) Representative SEM images of the strut cross sections and the corresponding elemental distribution of the PDLLA-Zn-nitrided BRS 1, 2, 3, 4, 6, 9, 12, 18, and 24 months postimplantation in rabbit abdominal aortas. (**B**) TEM image of the cross section of the PDLLA-Zn-nitrided Fe BRS strut and the corresponding elemental mapping 3 months postimplantation. (**C**) Morphology of the nanoscale Zn sacrificial layer region adjacent to the nitrided Fe platform and selected area electron diffraction (SAED) patterns of the marked regions (i) Fe, (ii) ZnO, and (iii) $\alpha - Zn_3(PO_4)_2$ 3 months postimplantation. (**D**) TEM image of the cross section of the PDLLA-Zn–nitride Fe BRS strut and the corresponding elemental mapping 24 months postimplantation. (**E**) Morphology of the biodegradation products in the residual strut and the corresponding SAED patterns of the marked regions (iv) Fe_3O_4, Fe_2O_3, and (v) $Fe_3(PO_4)_2$ 24 months postimplantation.

arrow) indicates the remaining dispersed biodegradation products of the nitrided Fe struts. No apparent lumen area loss was found at 6- and 26-month follow-up. The results of the first in-human implantation trial show a good safety profile, a promising angiographic performance, and an appropriate biodegradation behavior of the PDLLA-Zn-nitrided Fe BRS. The results of another case are shown in fig. S5, illustrating a similar biodegradation process of the scaffold.

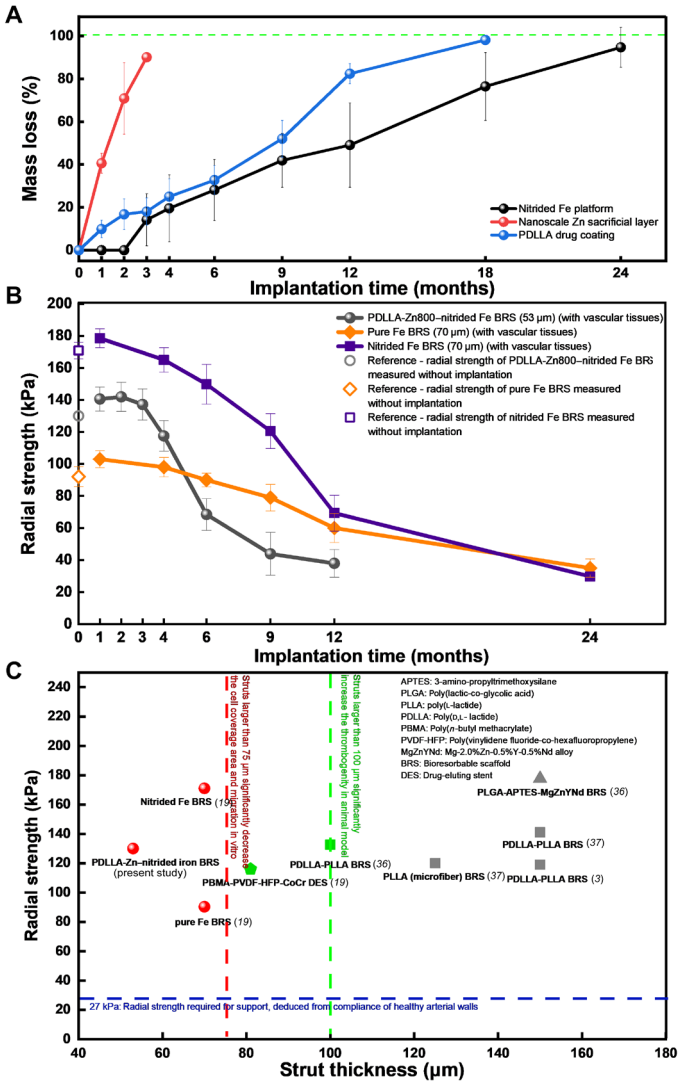

Fig. 4. Evolution of the PDLLA-Zn-nitrided Fe BRS in a rabbit abdominal aorta. (**A**) Mass loss of each layer after careful separation of the layers. The black line represents the mass loss of the nitrided Fe platform (obtained by weighing the remaining struts after removing the tissues and biodegradation products; $n = 11$), the red line represents the mass loss of the nanoscale Zn sacrificial layer (Zn in its elemental state; obtained using AAS; $n = 11$), and the blue line represents the mass loss of the PDLLA drug coating (obtained using gel permeation chromatography; $n = 11$) as a function of time point after BRS implantation. (**B**) Radial strength evolution of the PDLLA-Zn800-nitrided Fe BRS in the present study and the pure and nitrided Fe BRSs reported in our previous study (*19*) as a function of time point after implantation. The PDLLA-Zn800-nitrided Fe BRS's metallic strut was 53 μm thick, while the pure and nitrided Fe BRSs' metallic struts were 70 μm thick. The radial strength was measured with vascular tissues, except for the initial values ($n = 8$). (**C**) Summary of radial strength–strut thickness features of the scaffolds/stents. Simon *et al*. (*33*) has reported 75 μm (dashed line in red) as a critical strut thickness, above which the strut will affect the cell coverage and migration of endothelial cells in vitro. Kolandaivelu *et al*. (*22*), on the other hand, has reported 100 μm (dashed line in green) as a critical strut thickness value in animal models, with the risk of thrombogenicity increasing when the strut thickness is larger than such value. Twenty-seven kilopascal is considered a threshold of radial strength (which is required for support) deduced from the compliance of healthy arterial walls (*34*).

DISCUSSION

The current commercialized BRSs are polymer- and magnesium-based scaffolds. More or less, these BRSs exhibit nonideal biodegradation profiles, either too steep or too gradual, resulting in a premature rupture of the scaffold or long-term vessel caging. The present design of the PDLLA-Zn-nitrided Fe BRS features a nanoscale Zn sacrificial layer, adjusting the biodegradation profile to meet the requirement of providing sufficient and transient mechanical support to the target vessel. Detailed modeling of the full bioresorption process (including both the biodegradation process of the scaffolds and the bioresorption of the biodegradation products) of the three individual material parts of the PDLLA-Zn-nitrided Fe BRS is demonstrated in the "Bioresorption process of the individual material parts of the PDLLA-Zn-nitrided Fe BRS" section, whereas the tunability of the PDLLA-Zn-nitrided Fe BRS's biodegradation by changing the thickness of the Zn sacrificial layer and the comprehensive medical device performance of the PDLLA-Zn-nitrided Fe BRS in its entirety are demonstrated in the "Tunable multistage biodegradation sequence of the PDLLA-Zn-nitrided Fe BRS obtained by adjusting the thickness of the Zn sacrificial layer" and "Comprehensive medical device performance of the PDLLA-Zn-nitrided Fe BRS compared to that of the current commercial BRS" sections, respectively.

Bioresorption process of the individual material parts of the PDLLA-Zn-nitrided Fe BRS

The full bioresorption process of the scaffold includes both the biodegradation process of the scaffold materials in the physiological environment and the bioresorption of the biodegradation products by the surrounding tissues. We observed the full biodegradation process of the PDLLA-Zn-nitrided Fe BRS in rabbit abdominal aortas in the present study, and the results of our observation will be described in detail in this section. Full bioresorption of the PDLLA drug coating and Zn sacrificial layer was achieved, but full bioresorption of the nitrided Fe platform was not observed in the rabbit abdominal aorta at the 24-month monitoring end point and in the human coronary artery at the 26-month follow-up time point. As we observed numerous macrophages near the struts in the human artery, we could reasonably suppose that the nitrided Fe platform would be fully bioresorbed a few months thereafter in the human artery. It has been reported that nitrided Fe biodegradation products with low solubility can be cleared by macrophages (*19*). Briefly, insoluble biodegradation products will be engulfed by the macrophages around the struts, transformed into hemosiderin, and transferred to the adventitia. Last, the hemosiderin-laden macrophages will enter the lymphatics and will travel to the adjacent lymph nodes to finish the bioresorption process of the insoluble nitrided Fe biodegradation products. However, we hardly found macrophages near the struts in the rabbit abdominal aortas in this study, which could explain the absence of the bioresorption stage. In contrast, macrophages have been observed extensively near the struts in human and porcine arteries, and they have been found to play a role in the bioresorption of nitrided Fe biodegradation products, which is verified by fig. S6 and by the results of our previous study (*19*). On the basis of our observations in this and our previous studies, we show the full bioresorption process of the PDLLA-Zn-nitrided Fe BRS in different animal models and the human coronary artery in fig. S7. The biodegradation stage lasts for about 2 years in both the rabbit abdominal aorta and the human coronary artery while we assume

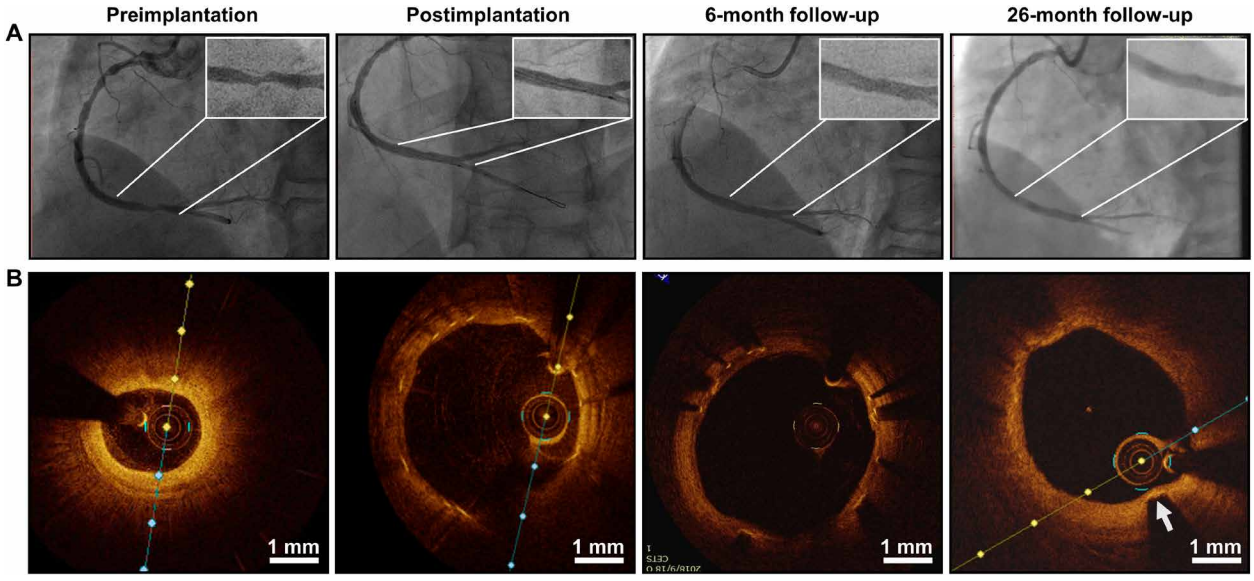

Fig. 5. First in-human implantation of the PDLLA-Zn-nitrided Fe BRS. (**A**) Angiographic appearance of the scaffolded vessel segment and (**B**) representative OCT images before the procedure, after scaffold implantation, and at 6- and 26-month follow-up.

that the biodegradation stage of the scaffold lasts much longer in the porcine coronary artery according to our previous studies (*19*, *21*). We observed the bioresorption of the biodegradation products by macrophages in the human and porcine coronary arteries, but we did not clearly observe the same in the rabbit abdominal aortas in the present study. Therefore, although the biodegradation products had remained in situ in the human coronary artery 26 months postimplantation, we could reasonably predict that the scaffold would be fully resorbed within the following months.

It deserves mention that in this study, we chose to implant the PDLLA-Zn-nitrided Fe BRS in rabbit abdominal aortas rather than in porcine coronary arteries because the degradation in the rabbit abdominal aorta is faster than that in the porcine coronary artery within the first 6 months, and faster degradation usually corresponds to a higher risk. We used the rabbit model as the worst case for preclinical evaluation. The low cost of the rabbit model compared with the porcine model was also an advantage. With these considerations, we chose the rabbit model for the systematic investigation of the in vivo degradation behavior of the PDLLA-Zn-nitrided Fe BRS.

PDLLA drug coating

As shown in Fig. 6A, the PDLLA drug coating undergoes bulk erosion. Upon implantation, water molecules penetrate the coating, a process called incubation (stage i in Fig. 6A). After several hours of penetration, the ester bonds start to cleave, and hydrolysis occurs. At the second stage, termed induction (stage ii in Fig. 6A), the hydrolysis continues, with no apparent weight loss observed. Erosion and bioresorption (stage iii in Fig. 6A) start within a month after implantation and go on for about 18 months, until the PDLLA drug coating is completely biodegraded and bioresorbed. At stage iii, soluble oligomers are formed, are diffused into the surrounding vascular tissues, and are finally metabolized into CO_2 and H_2O. This process is also revealed by the molecular weight evolution of the PDLLA drug coating (fig. S8). The hydrolyzed hydrogen ions lead to a lower pH value in the coating, while the simultaneous biodegradation of zinc/iron is helpful for neutralizing the local pH in the surrounding tissue, potentially relieving the inflammation.

Nanoscale Zn sacrificial layer

As shown in Fig. 6B, the nanoscale Zn sacrificial layer undergoes corrosion-based biodegradation. It remains intact within the first several hours (stage i in Fig. 6B) after the implantation of the PDLLA-Zn-nitrided Fe BRS into the blood vessel. The Zn sacrificial layer is biodegraded when the water molecules and other inorganic/organic groups in the plasma penetrate the PDLLA drug coating and reach the surface of the nanoscale Zn sacrificial layer. The biodegradation of the Zn sacrificial layer goes on for about 3 months (stage ii in Fig. 6B), and by the end of this stage, the metallic Zn will have been completely transformed into its biodegradation products. Thereafter, the zinc biodegradation products will undergo bioresorption for another 3 months (stage iii in Fig. 6B), as revealed by the variation of the Zn^{2+} concentration of the ions in the surrounding vascular tissues at the different time points after implantation in fig. S1. The bioresorption stage partially overlaps the biodegradation stage. The corresponding chemical reactions during the biodegradation of the zinc sacrificial layer are discussed in detail herein. The zinc layer first undergoes biodegradation with the anodic reaction of zinc dissolution and the cathodic reaction of oxygen reduction, as shown below

$$\text{Anodic reaction: } Zn \rightarrow Zn^{2+} + 2e^- \quad (1)$$

$$\text{Cathodic reaction: } O_2 + 2H_2O + 4e^- \rightarrow 4OH^- \quad (2)$$

$$\text{Overall reaction: } Zn^{2+} + 2OH^- \rightleftharpoons Zn(OH)_2 \quad (3)$$

$$Zn^{2+} + 2OH^- \rightleftharpoons ZnO + H_2O \quad (4)$$

With the biodegradation of the Zn sacrificial layer, the local pH increases, leading to the formation of $Zn(OH)_2$/ZnO, where ZnO is more stable than $Zn(OH)_2$, as we found in our recent study on the pure Zn bare scaffold (*25*). The increase of the local pH also accelerates the hydrolysis of the PDLLA coating at the interface, which provides more ─COOH end groups, interacting with OH^-. Therefore, as indicated by TEM (Fig. 3C) and the Pourbaix diagram (fig. S9), with decreasing pH, ZnO gradually dissolves and transforms into $Zn_3(PO_4)_2$ in the reaction shown below

$$3Zn^{2+} + 2HPO_4^- + 2OH^- \rightleftharpoons Zn_3(PO_4)_2 + 2H_2O \quad (5)$$

$Zn_3(PO_4)_2$ has been widely used in antirust paints, and its anticorrosion effect has been reported (*26*–*28*). Therefore, apart from the sacrificial protection by metallic Zn when coupling with the nitrided Fe platform, the biodegradation products of the Zn sacrificial layer also act as physical barriers, preventing the biodegradation of the nitrided Fe platform (termed inhibitory protection).

Nitrided Fe platform

As shown in Fig. 6C, the nitrided Fe platform underwent biodegradation, and the whole process was divided into several stages. Before the onset of biodegradation, the nitrided Fe platform went through two incubation stages: incubation of the PDLLA drug coating (stage i in Fig. 6C) and incubation of the Zn sacrificial layer (stage ii in Fig. 6C). The former lasted for several hours, and the latter lasted for months, until the area coverage ratio of the nanoscale zinc sacrificial layer on the nitrided Fe platform was already so low that it could no longer effectively protect the nitrided Fe platform through the galvanic mechanism. Afterward, the nitrided Fe platform started to degrade, and it gradually transformed into biodegradation products in about 21 months in the rabbit abdominal aorta models (stages iii to v in Fig. 6C). At stage iii, as shown in Fig. 6C, the biodegradation of the nitrided Fe platform became rapid due to the presence of the PDLLA coating and its acidic hydrolysis products. The biodegradation rate slowed down when a thick biodegradation product layer of the nitrided Fe platform was formed (stage iv in Fig. 6C). At 18 months after implantation, when the PDLLA drug coating had been completely hydrolyzed, we found the nitrided Fe platform directly exposed to the vascular matrix, and we found Ca/P deposition on the surfaces of the nitrided Fe platform struts (stage v in Fig. 6C). By 24 months, the nitrided Fe platform had been completely degraded. Partially overlapped with the biodegradation process, it went into the stage (stage vi in Fig. 6C) where its various biodegradation products were bioresorbed and transported, which lasted for several months.

The corresponding chemical reactions during the biodegradation of the nitrided Fe platform (stages iii to v in Fig. 6C) can be demonstrated as follows. First, in the presence of water and dissolved oxygen in body fluid, the biodegradation of nitrided Fe proceeds according to the electrochemical reactions (Eqs. 2 and 6). These reactions lead to the deposition of $Fe(OH)_2$ (Eq. 7), which is further oxidized to magnetite and ferrous hydroxide, as depicted in Eqs. 8 and 9, respectively. According to the TEM results in the present study, Fe_2O_3 and FeOOH were also among the biodegradation products of the nitrided Fe platform 12 and 24 months postimplantation, which could be attributed to the dehydration of $Fe(OH)_3$, as indicated in both Eqs. 10 and 11

$$\text{Anodic reaction: } Fe \rightarrow Fe^{2+} + 2e^- \quad (6)$$

Cathodic reaction: same as Eq. 2

$$Fe^{2+} + 2OH^- \leftrightarrow Fe(OH)_2 \quad (7)$$

$$3Fe(OH)_2 + \frac{1}{2}O_2 \longrightarrow Fe_3O_4 + 3H_2O \quad (8)$$

$$2Fe(OH)_2 + \frac{1}{2}O_2 + H_2O \longrightarrow 2Fe(OH)_3 \quad (9)$$

$$Fe(OH)_3 \longrightarrow FeOOH + H_2O \quad (10)$$

$$2Fe(OH)_3 \longrightarrow Fe_2O_3 + 3H_2O \quad (11)$$

Another biodegradation product of the nitrided Fe platform that we found in the present study was ferrous phosphate, which was formed by the diffusion of the iron ions released from the nitrided Fe platform toward the interface between the biodegradation products of the nitrided Fe platform and the PDLLA drug coating undergoing biodegradation, while phosphate and oxygen diffused in opposite directions, from the interstitial fluid into the PDLLA drug coating. The chemical reaction of ferrous phosphate formation is depicted in Eq. 12

$$3Fe^{2+} + 2HPO_4^{2-} \longrightarrow Fe_3(PO_4)_2 + 2H^+ \quad (12)$$

We found both Fe_2O_3 and Fe_3O_4 at the center of the intact nitrided Fe platform, while we found $Fe_3(PO_4)_2$ only at the outer layer of the nitrided Fe platform. Some ferrous ions diffused into the surrounding tissues and were mainly present in situ as α-FeOOH and γ-FeOOH phases (fig. S2).

Tunable multistage biodegradation sequence of the PDLLA-Zn-nitrided Fe BRS obtained by adjusting the thickness of the Zn sacrificial layer

As shown in fig. S4 and table S1, the previous pure Fe BRS, nitrided Fe BRS, and PDLLA-nitrided Fe BRS exhibit a single-stage biodegradation profile, with biodegradation of the Fe/nitrided Fe platform starting right after implantation. The pure Fe BRS and the nitrided Fe BRS slowly degrade during the whole biodegradation period (*19*), while the application of the PDLLA coating excessively accelerates the biodegradation process, which may result in the premature rupture of the scaffold. The intercalated design of a nanoscale Zn sacrificial layer with an adjustable thickness delays the onset of biodegradation of the nitrided Fe platform and realizes the tunable multistage biodegradation function of the PDLLA-Zn-nitrided Fe BRS, with the detailed mechanism being revealed in Fig. 6D. The Zn sacrificial layer starts to degrade after the incubation stage of the PDLLA drug coating, forming a thin layer of zinc biodegradation product (τ_1 stage). As the thickness of the Zn sacrificial layer is very low (nanoscale), the Zn sacrificial layer will open soon after the onset of Zn biodegradation, and the underlying nitrided Fe platform will be exposed. At this stage (τ_2 stage), metallic Zn, as an anode, forms a galvanic couple with the underlying nitrided Fe platform and provides sacrificial protection. The biodegradation products will then cover the openings. The zinc biodegradation products can also provide inhibitory protection to the underlying nitrided Fe platform at the subsequent stage (τ_3 stage). It is generally recognized that about 90% consumption of the Zn layer provides sacrificial protection via

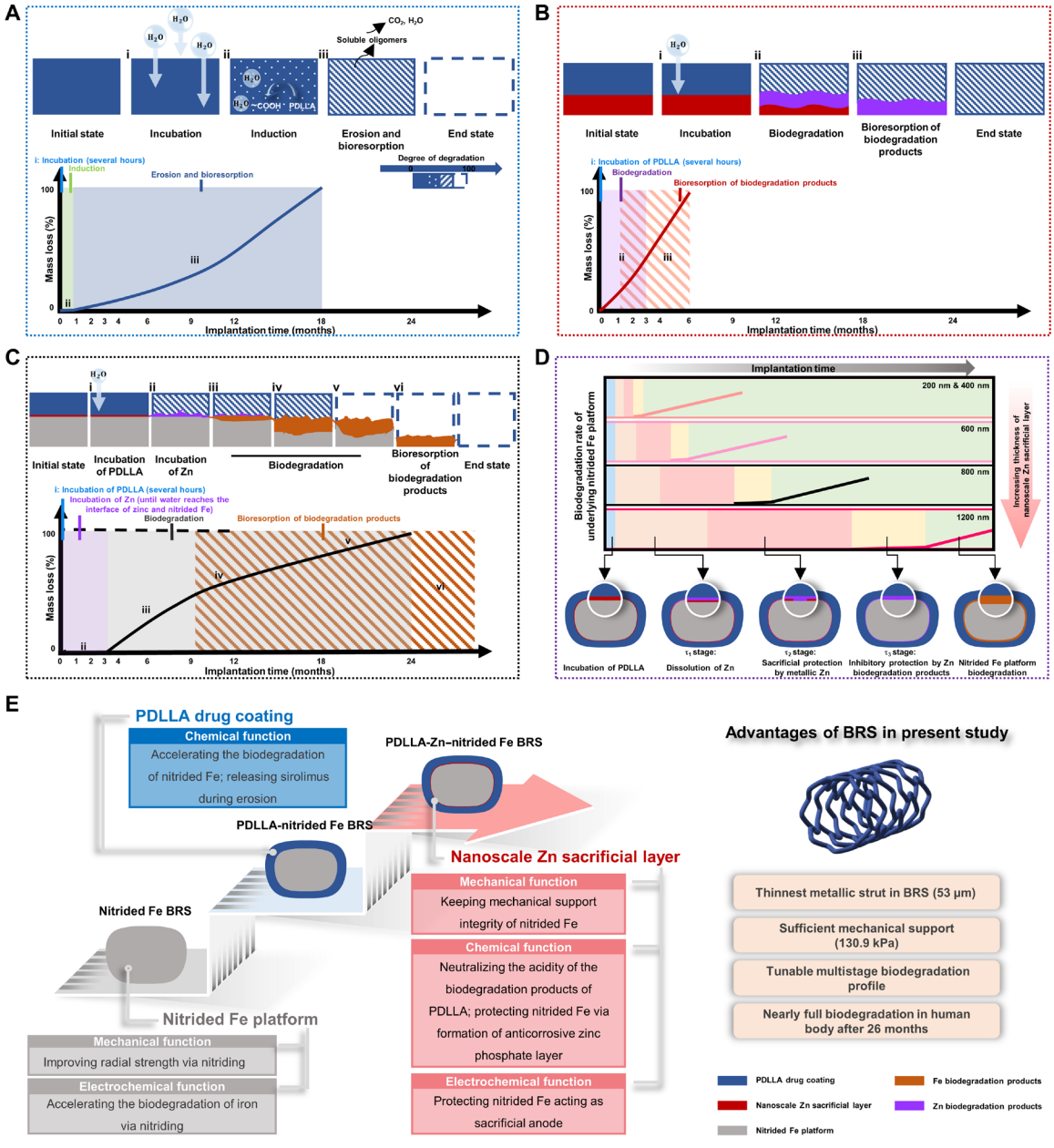

Fig. 6. Schematic diagram of the full bioresorption process and functions of different parts of the PDLLA-Zn-nitrided Fe BRS, with the PDLLA-Zn800–nitirded Fe BRS as an example. (**A**) Full bioresorption process of the PDLLA drug coating with three stages: incubation, induction, and erosion and bioresorption. (**B**) Full bioresorption process of the nanoscale Zn sacrificial layer with three stages: PDLLA incubation stage, zinc biodegradation stage, and bioresorption of biodegradation products stage. (**C**) Full bioresorption process of the nitrided Fe platform with four stages: incubation of the PDLLA coating, incubation of the Zn sacrificial layer, biodegradation stage, and bioresorption of biodegradation products stage. The biodegradation stage of the nitrided Fe platform can be further divided into three substages in terms of the evolution of its degradation microenvironment: waterish PDLLA coating with or without partial protection by the zinc biodegradation products and direct contact with the vascular tissue. After complete biodegradation of the nitrided Fe platform, its biodegradation products gradually dissolve into the surrounding tissues and be engulfed by macrophages. (**D**) Tunable multistage biodegradation function of the scaffold realized via intercalation of the nanoscale Zn sacrificial layer with an adjustable thickness. (**E**) Comprehensive technical advantages of the PDLLA-Zn-nitrided Fe BRS.

anodic galvanic corrosion, while the remaining 10% undergoes self-corrosion and the zinc biodegradation products provide inhibitory protection to the underlying platform (*29*). The duration of the protective stage, including the τ_1, τ_2, and τ_3 stages, shows a positive relation with the thickness of the Zn sacrificial layer. As shown in Fig. 6D and fig. S4, for the PDLLA-Zn-nitrided Fe BRS, if the thickness of the Zn sacrificial layer is no more than 400 nm, then its protection of the nitrided Fe platform is negligible, and the duration of the protective stage ($\tau_1 + \tau_2 + \tau_3$) is much less than 1 month. The nitrided Fe platforms in the PDLLA-Zn-nitrided Fe BRSs with 600-, 800-, and 1200-nm-thick Zn sacrificial layers, respectively, can be kept intact for 1, 2, and 6 months in a rabbit abdominal aorta,

indicating a longer duration of the protective stage with a thicker Zn sacrificial layer. In summary, the introduction of a nanoscale Zn sacrificial layer between the PDLLA coating and the nitrided Fe platform can protect the nitrided Fe platform (whose protection period varies with its thickness) from early overcorrosion. After the consumption of the Zn sacrificial layer, the nitrided Fe platform degrades rapidly in the acidic microenvironment provided by the PDLLA coating, which is desirable especially when the blood vessel remodeling has been finished.

It is of note that the presence of a nanoscale Zn sacrificial layer delays the onset of nitrided Fe platform biodegradation and helps regulate the whole biodegradation period of the PDLLA-Zn-nitrided Fe BRS. The "acid" biodegradation products of the PDLLA drug coating seem to accelerate the biodegradation of the nitrided Fe platform, whereas the nanoscale Zn layer delays such biodegradation either as a "sacrificial anode" to completely protect the nitrided Fe platform or by neutralizing the acidity of the biodegradation products of the PDLLA drug coating through its alkaline biodegradation products. The combination of a PDLLA drug coating and a nanoscale Zn sacrificial layer makes the biodegradation behavior of the PDLLA-Zn-nitrided Fe BRS multistage, and the duration of each stage can be regulated/programmed to prevent the immature degeneration of the mechanical support at the initial stage and the long-term retention of the scaffold in the body after the repair of the scaffolded blood vessel.

Comprehensive medical device performance of the PDLLA-Zn-nitrided Fe BRS compared to that of the current commercial BRS

The optimal combination of the three different parts of the present PDLLA-Zn-nitrided Fe BRS endows such BRS with multiple advantages, as shown in Fig. 6E. First, unlike simple Fe, the nitrided Fe platform largely enhances the radial strength of the scaffold and exhibits a faster biodegradation rate. Second, the PDLLA drug coating serving as a drug carrier can release sirolimus at a reasonable rate through its erosion, and it can accelerate the biodegradation of the nitrided Fe platform by providing an acidic microenvironment. Third, the presence of a nanoscale Zn sacrificial layer can protect the nitrided Fe platform from biodegradation by acting as a sacrificial anode and forming an anticorrosive zinc phosphate layer, which will help keep the mechanical integrity of the scaffold at the early stage. Moreover, it can neutralize the acidity of the biodegradation products of the PDLLA drug coating, leading to less inflammation. Hence, the PDLLA-Zn-nitrided Fe BRS has the mechanical property and biodegradation behavior required for a promising BRS. Benefiting from this, the PDLLA-Zn-nitrided Fe BRS showed superior efficacy and excellent biocompatibility in rabbit abdominal aortas. Rapid endothelialization was observed, and the coverage ratio above the struts reached 94.85% 28 days postimplantation, much higher than that with other BRSs and DESs (fig. S10, A and B, and table S2). Besides, as early as 14 days postimplantation, most of the struts were covered with neointimal tissue, and no apparent increase in neointimal thickness was observed with time point after implantation (fig. S10C). We did not observe any peeling of the PDLLA drug coating 28 days postimplantation, when the endothelialization had been completed (fig. S11). Furthermore, the PDLLA-Zn-nitrided Fe BRS scaffolded vessels showed mild inflammation, indicating better biocompatibility than the current BRSs [inflammation score (90 days): 1.09 for the PDLLA-Zn-nitrided Fe BRS (*21*) versus 1.67 for Magmaris (*30*) in the porcine model], but the inflammation was relieved with time (table S2). There was no pathological change in main tissues (fig. S12). Although the healthy rabbit abdominal model cannot fully reflect a diseased human coronary artery where atherosclerotic plaques exist, it appears to indicate relative safety during the biodegradation process of the scaffold. First, the developed neointima after a BRS implantation could transform unstable plaques to more stable ones, largely reducing inflammation risks. Besides, the released sirolimus with PDLLA hydrolysis could also significantly relieve inflammation. Therefore, we expect similar scaffold biodegradation with mild inflammation upon real-world condition. Quite encouragingly, as mentioned above, our first in-human implantation also achieved a good safety profile and a promising angiographic performance. The PDLLA-Zn-nitrided Fe BRS in the present study loads sirolimus (6.1 μg/mm dose), a common antiproliferative drug, and its drug release profile has been studied (fig. S13). Such BRS's drug release can be well controlled by a mature technology and is almost not influenced by the biodegradation of the zinc sacrificial layer and the nitrided Fe platform.

To summarize, the present PDLLA-Zn-nitrided Fe BRS with a distinctive intercalated structure design exhibits the preferred mechanical properties and biodegradation behavior for clinical application. The metallic strut thickness of the PDLLA-Zn-nitrided Fe BRS was reduced to 53 μm, much lower than those of the other BRSs (e.g., 150 μm for Absorb BVS and Magmaris) and even lower than those of the mainstream DESs (e.g., 81 μm for Xience Prime), which can facilitate endothelialization and reduce thrombosis. Despite its thin strut, the PDLLA-Zn-nitrided Fe BRS has sufficient mechanical support, with 131-kPa radial strength. The intercalated design of the scaffold alters the biodegradation behavior of the nitrided Fe platform to a multistage mode, keeping the platform intact within the first several months after BRS implantation under the protection of the nanoscale Zn sacrificial layer and then allowing it to undergo gradual biodegradation due to the presence of a PDLLA coating. Moreover, the duration of each stage is tunable by adjusting the thickness of the nanoscale Zn sacrificial layer to make it match the remodeling duration of the scaffolded blood vessel. In this study, we observed the complete biodegradation of the PDLLA-Zn-nitrided Fe BRS 24 months after implantation in the rabbit abdominal aorta and nearly complete biodegradation 26 months after implantation in the human coronary artery. However, our study can still be improved by addressing the following issues: (i) The time point of the full resorption of the PDLLA-Zn-nitrided Fe BRS without any leftover biodegradation product was not provided; and (ii) only two cases of implantation in human coronary artery was presented (the first in-man trial with 65 enrolled patients is still in progress), and a randomized controlled trial is needed for a robust evaluation of the PDLLA-Zn-nitrided Fe BRS's safety and efficacy.

MATERIALS AND METHODS

Study design

The main objective of the study was to investigate the in vivo degradation behavior of the PDLLA-Zn-nitrided Fe BRS, covering its total biodegradation cycle. We placed PDLLA-Zn-nitrided Fe BRSs in the abdominal aortas of adult New Zealand white rabbits and then performed macroscopic observation through optical images, 3D reconstruction micro-CT images, and mass loss measurement. We obtained the microscopic appearance of the scaffold via SEM and TEM.

The sample size power calculations were not well defined; hence, the sample size power must be estimated. Typically, 10 to 12 test BRS formulations per time point are satisfactory according to the consensus-based recommendations (*31*). At each time point, we explanted the scaffolded vessels for characterization. We purchased adult New Zealand white rabbits (mean weight, 2.0 kg; range, 1.6 to 2.4 kg) from Pearl Laboratory Animal Science and Technology Co. Ltd. (Guangdong, China) and fed them with a standard diet without cholesterol lipid supplementation throughout the experiment. We did not eliminate any outliers in the study. The animal experiments in this study were approved for use by the Institutional Animal Ethics Committee of Shenzhen Testing Center of Medical Devices.

We conducted pooled analysis after collecting follow-up data. For the PDLLA-Zn-nitrided Fe BRS, the PDLLA coating mass loss results included the data at 1 month (N = 3), 2 months (N = 2), 3 months (N = 3), 4 months (N = 2), 6 months (N = 1), 9 months (N = 2), 12 months (N = 1), and 18 months (N = 1) postimplantation; the Zn sacrificial layer mass loss results included the data at 1 month (N = 10; n = 11), 2 months (N = 10; n = 11), and 3 months (N = 7; n = 11) postimplantation; and the nitrided Fe platform mass loss results included the data at 1 month (N = 10; n = 11), 2 months (N = 9; n = 11), 3 months (N = 7; n = 11), 4 months (N = 5; n = 11), 6 months (N = 9; n = 11), 9 months (N = 6; n = 11), 12 months (N = 9; n = 11), 18 months (N = 5; n = 11), and 24 months (N = 7; n = 11) postimplantation. The radial strength results included the data at 1 month (N = 3; n = 8), 2 months (N = 5; n = 8), 3 months (N = 4; n = 8), 4 months (N = 3; n = 8), 6 months (N = 4; n = 8), 9 months (N = 5; n = 8), and 12 months (N = 3; n = 8) postimplantation. The molecular weight evolution of the PDLLA drug coating with time point after implantation included the data at 1 month (N = 4), 2 months (N = 3), 3 months (N = 4), 4 months (N = 3), 6 months (N = 4), 9 months (N = 2), and 12 months (N = 1) postimplantation. Note that to measure the molecular weight and mass loss of the PDLLA drug coating, we implanted three PDLLA-Zn-nitrided Fe BRSs in each rabbit. Then, at each time point, we explanted the scaffolds, dissolved their PDLLA drug coatings, and combined the PDLLA solutions from the same rabbit for measurement because the amount of PDLLA drug coating of a single scaffold was too small to measure. Therefore, we obtained only one combined result from the scaffolds collected from each rabbit.

Scaffold fabrication and characterization

The nitrided Fe-based BRSs with a nanoscale Zn sacrificial layer and a PDLLA drug coating (PDLLA-Zn-nitrided Fe BRS) that we used in this study were fabricated by Lifetech Scientific Co. Ltd. (Shenzhen, China). Briefly, high-purity iron tubes were used as the starting materials. These tubes were fabricated into iron scaffolds through plasma nitriding, tube drawing, laser cutting, chemical etching, and electropolishing, in sequence. Zinc was deposited on the surface of the nitrided Fe platform through electroplating, after which sirolimus-carrying amorphous PDLLA (Evonik Industries, Germany) coating was applied through ultrasonic atomization spraying. All the scaffolds were crimped onto matching rapid exchange balloon catheters (Φ3.0 × 8 mm; Lifetech Scientific, Shenzhen, China). Last, sterilization was conducted before the experiments.

After depositing a nanoscale zinc sacrificial layer, we used an x-ray diffractometer (DMAX 2400, Rigaku, Japan) with Cu Kα radiation to detect the composition of the samples. The scan rate was 4°/min. To characterize the surface chemistry, we conducted XPS (Axis Ultra DLD, SHIMADZU, Japan). We also characterized the PDLLA drug coating via FTIR (Nicolet 6700, Thermo Fisher Scientific, USA). After embedding the PDLLA-Zn-nitrided Fe BRSs in resin, we observed the cross-sectional morphology of the strut via SEM (JSM-6510, JEOL, Japan) operated at 10-kV accelerating voltage.

Animal surgical procedure

We placed PDLLA-Zn-nitrided Fe BRSs (Φ3.0 × 8 mm) in the abdominal aortas of adult New Zealand white rabbits after anesthetizing them with 0.3% sodium pentobarbital through intravenous injection. For each rabbit, we surgically exposed the right femoral artery and introduced a 5F guide catheter over a 0.014-inch (0.3556-mm) micro guidewire. At the same time, we gave each rabbit heparin sodium (200 U/kg) intravenously to prevent thrombosis. Then, we introduced and positioned the scaffold in the abdominal aorta under fluoroscopic control. We inflated a balloon with 8 atm (nominal pressure) to 10 atm for 30 s for deploying the scaffold, and we took care to avoid placing the scaffold across the orifice of the major branches of the descending aorta. We then deflated the balloon, removed the guidewire, and carefully sutured the puncture site. We gave each rabbit 16×10^5 U of penicillin intramuscularly.

Qualitative characterization of in vivo degradation through micro-CT analysis

At each time point, we sacrificed rabbits and carefully dissected the scaffolded artery segments. We scanned the scaffolds with vessel tissues through high-resolution micro-CT (Skyscan1172, Bruker, Germany) and conducted 3D reconstruction to analyze the scaffold degradation extent.

Mass loss measurement

After carefully separating the layers, we quantitatively measured the in vivo degradation behaviors via atomic absorption spectroscopy (AAS) and the mass loss method. We carefully separated the vessel tissues from the scaffolds and dissolved them through microwave nitrification. Then, we filtered the solution and fixed the volume. We measured the Zn concentration in the tissues via AAS (Spectra AA240FS, Agilent, USA). After removing the tissues, we immersed the scaffolds in ethyl acetate ($CH_3COOC_2H_5$) under ultrasound for 20 min to separate the PDLLA coating from the matrix. We used PDLLA-$CH_3COOC_2H_5$ solution to test the quality of PDLLA via gel permeation chromatography coupled with multiangle laser light scattering (GCP-MALLS) with an Agilent PLgel MIXED-C column, an Agilent G1329 autosampler, a Wyatt Optilab T-rEX differential refractometer, and a Wyatt DAWN 8+ eight-angle laser light scattering detector. To measure the molecular weight of the PDLLA drug coating, we used tetrahydrofuran to dissolve the coating and measure the molecular weight using GCP-MALLS. We immersed the remaining scaffolds in saturated glycine solution under ultrasound for 10 s and then washed them with water and ethanol. We then immersed the remaining scaffolds in NaOH (1 M) solution for 10 to 20 min to dissolve the zinc on the iron surface. We also measured the zinc concentration in the NaOH solution via AAS (Spectra AA240FS, Agilent, USA) to determine the remaining Zn amount.

After immersing the scaffolds in NaOH, we immersed them in tartaric acid (3 weight %) under ultrasound for 20 min to remove the biodegradation products from their struts. We cleaned the remaining

scaffold struts with NaOH (1 M), deionized water, and absolute ethyl alcohol, in sequence, and then weighed the dried nitrided Fe platform and calculated the biodegradation rate via the mass loss method.

Biodegradation product characterization via SEM/TEM

We prepared hard tissue slices of the scaffolds dissected from the sacrificed rabbits as described in our previous work (*18*). Briefly, we collected the scaffolded arteries and embedded them in methyl methacrylate. We then prepared cross-sectional samples by cutting the embedded tissues into 1- to 1.5-mm-thick slices, successively grinding the slices with 1200, 2000, and 7000 grit SiC paper, and polishing them with a water-soluble 0.5-μm diamond slurry on microfiber. Thereafter, we observed the morphology of the strut cross section and the corresponding elemental distribution via SEM (JSM-6510, JEOL, Japan) and EDS (Oxford Inca Energy 350, Oxford Instruments, UK). Besides, we chose microstructures of the biodegradation products and representative areas for further identification via field emission gun TEM (JEM-2100F, JEOL, Japan) after sample preparation via focused ion beam (FIB; GAIA3, Tescan, Czech Republic).

Radial strength measurement

Using a radial strength tester (RX550-100, Machine Solution Inc., USA) with a 0.1 mm/s of compression rate, we measured the radial strength of the scaffolds with vessel tissues dissected from the sacrificed rabbits. We defined the strength at 10% compression of the original scaffold's outer diameter as the radial strength (kilopascal).

Histological analysis

We fixed the segments of the scaffolded artery dissected from the sacrificed rabbits with 4% (w/v) paraformaldehyde and then dehydrated them and embedded them in paraffin. Then, we stained the sections with H&E and Masson's trichrome. Thereafter, we observed the local-tissue response and the biodegradation products of the scaffolds using a biological microscope (DM2500, Leica, Germany).

Evaluation of the scaffold endothelialization

To characterize the endothelialization after implantation, we collected segments of the scaffolded arteries and cut them in the middle, along the long axis. We then took different magnification images of the iliac artery scaffold of the rabbits 28 days after implantation via SEM (JEOL 6510, Japan). In addition, we conducted confocal laser scanning microscopy and dual immunofluorescent staining of p120 (green channel) and vascular endothelial (VE)–cadherin (red channel) with 4′,6-diamidino-2-phenylindole counterstain (blue channel) to evaluate the endothelialization of the scaffold. We visually estimated the extent of endothelial coverage based on the positive signals of the p120/VE-cadherin colocalized markers above the struts and expressed this as a mean percentage of the total area above the scaffold struts for the entire scaffolded surface.

First in-human implantation

A 60-year-old man underwent percutaneous coronary intervention for target stenosis (80%) in the distal right coronary artery with the standard international techniques. The procedure was carried out at Fuwai Hospital (Beijing, China) and was transmitted live to China Interventional Therapeutics Conference 2018 (23 March 2018) (*32*) after the patient's informed consent for such was obtained. A Φ3.5 × 18 mm PDLLA-Zn-nitrided Fe BRS was implanted in the target lesion of the right coronary artery via the conventional stenting technique and the right radial artery approach. Coronary angiography and OCT (OPTIS, Abbott, USA) imaging were performed before and after implantation, at 6-month (18 September 2018) and 26-month (10 June 2020) follow-up. The patient was required to receive 100 mg of aspirin daily for the study duration and 75 mg of clopidogrel daily for a minimum of 12 months. The clinical study of the first in-human implantation of the PDLLA-Zn-nitrided Fe BRS was approved by the Ethics Committee of Fuwai Hospital, China.

Statistical analysis

We used descriptive statistical methods to present the data we had collected from different rounds of animal experiments. We expressed all the statistical data as means ± SD.

SUPPLEMENTARY MATERIALS

Supplementary material for this article is available at http://advances.sciencemag.org/cgi/content/full/7/23/eabf0614/DC1

View/request a protocol for this paper from *Bio-protocol*.

REFERENCES AND NOTES

1. J. Iqbal, Y. Onuma, J. Ormiston, A. Abizaid, R. Waksman, P. Serruys, Bioresorbable scaffolds: Rationale, current status, challenges, and future. *Eur. Heart J.* **35**, 765–776 (2014).
2. Y. Onuma, P. W. Serruys, Bioresorbable scaffold: The advent of a new era in percutaneous coronary and peripheral revascularization? *Circulation* **123**, 779–797 (2011).
3. C. Indolfi, S. De Rosa, A. Colombo, Bioresorbable vascular scaffolds–basic concepts and clinical outcome. *Nat. Rev. Cardiol.* **13**, 719–729 (2016).
4. P. W. Serruys, J. A. Ormiston, Y. Onuma, E. Regar, N. Gonzalo, H. M. Garcia-Garcia, K. Nieman, N. Bruining, C. Dorange, K. Miquel-Hébert, S. Veldhof, M. Webster, L. Thuesen, D. Dudek, A bioabsorbable everolimus-eluting coronary stent system (ABSORB): 2-year outcomes and results from multiple imaging methods. *Lancet* **373**, 897–910 (2009).
5. M. Haude, R. Erbel, P. Erne, S. Verheye, H. Degen, D. Böse, P. Vermeersch, I. Wijnbergen, N. Weissman, F. Prati, R. Waksman, J. Koolen, Safety and performance of the drug-eluting absorbable metal scaffold (DREAMS) in patients with de-novo coronary lesions: 12 month results of the prospective, multicentre, first-in-man BIOSOLVE-I trial. *Lancet* **381**, 836–844 (2013).
6. H. Jinnouchi, A. Sakamoto, S. Torii, F. D. Kolodgie, R. Virmani, A. V. Finn, Fully bioresorbable vascular scaffolds: Lessons learned and future directions. *Nat. Rev. Cardiol.* **16**, 286–304 (2019).
7. J. A. Ormiston, P. W. Serruys, E. Regar, D. Dudek, L. Thuesen, M. W. I. Webster, Y. Onuma, H. M. Garcia-Garcia, R. McGreevy, S. Veldhof, A bioabsorbable everolimus-eluting coronary stent system for patients with single de-novo coronary artery lesions (ABSORB): A prospective open-label trial. *Lancet* **371**, 899–907 (2008).
8. G. W. Stone, R. Gao, T. Kimura, D. J. Kereiakes, S. G. Ellis, Y. Onuma, W.-F. Cheong, J. Jones-Mcmeans, X. Su, Z. Zhang, P. W. Serruys, 1-year outcomes with the Absorb bioresorbable scaffold in patients with coronary artery disease: A patient-level, pooled meta-analysis. *Lancet* **387**, 1277–1289 (2016).
9. M. J. Lipinski, R. O. Escarcega, N. C. Baker, H. A. Benn, M. A. Gaglia Jr., R. Torguson, R. Waksman, Scaffold thrombosis after percutaneous coronary intervention with ABSORB Bioresorbable Vascular Scaffold: A Systematic review and meta-analysis. *JACC Cardiovasc. Interv.* **9**, 12–24 (2016).
10. J. J. Wykrzykowska, R. P. Kraak, S. H. Hofma, R. J. van der Schaaf, E. K. Arkenbout, A. J. IJsselmuiden, J. Elias, I. M. van Dongen, R. Y. G. Tijssen, K. T. Koch, J. Baan Jr., M. M. Vis, R. J. de Winter, J. J. Piek, J. G. P. Tijssen, J. P. S. Henriques; AIDA Investigators, Bioresorbable scaffolds versus metallic stents in routine PCI. *N. Engl. J. Med.* **376**, 2319–2328 (2017).
11. R. Erbel, C. Di Mario, J. Bartunek, J. Bonnier, B. de Bruyne, F. R. Eberli, P. Erne, M. Haude, B. Heublein, M. Horrigan, C. Ilsley, D. Böse, J. Koolen, T. F. Lüscher, N. Weissman, R. Waksman; PROGRESS-AMS (Clinical Performance and Angiographic Results of Coronary Stenting with Absorbable Metal Stents) Investigators, Temporary scaffolding of coronary arteries with bioabsorbable magnesium stents: A prospective, non-randomised multicentre trial. *Lancet* **369**, 1869–1875 (2007).
12. M. Haude, H. Ince, A. Abizaid, R. Toelg, P. A. Lemos, C. von Birgelen, E. H. Christiansen, W. Wijns, F.-J. Neumann, C. Kaiser, E. Eeckhout, S. T. Lim, J. Escaned, H. M. Garcia-Garcia,

R. Waksman, Safety and performance of the second-generation drug-eluting absorbable metal scaffold in patients with de-novo coronary artery lesions (BIOSOLVE-II): 6 month results of a prospective, multicentre, non-randomised, first-in-man trial. *Lancet* **387**, 31–39 (2016).
13. M. Haude, H. Ince, A. Abizaid, R. Toelg, P. A. Lemos, C. von Birgelen, E. H. Christiansen, W. Wijns, F.-J. Neumann, C. Kaiser, E. Eeckhout, S. T. Lim, J. Escaned, Y. Onuma, H. M. Garcia-Garcia, R. Waksman, Sustained safety and performance of the second-generation drug-eluting absorbable metal scaffold in patients with de novo coronary lesions: 12-month clinical results and angiographic findings of the BIOSOLVE-II first-in-man trial. *Eur. Heart J.* **37**, 2701–2709 (2016).
14. Coronary Resorbable Magnesium Scaffold (RMS) - Magmaris (2019); www.biotronik.com/en-de/products/coronary/magmaris.
15. M. Sabaté, F. Alfonso, A. Cequier, S. Romaní, P. Bordes, A. Serra, A. Iñiguez, P. Salinas, B. G. del Blanco, J. Goicolea, R. Hernández-Antolín, J. Cuesta, J. A. Gómez-Hospital, L. Ortega-Paz, J. Gomez-Lara, S. Brugaletta, Magnesium-based resorbable scaffold bersus permanent netallic sirolimus-eluting stent in patients with ST-segment elevation myocardial infarction: The MAGSTEMI randomized clinical trial. *Circulation* **140**, 1904–1916 (2019).
16. M. Peuster, P. Wohlsein, M. Brügmann, M. Ehlerding, K. Seidler, C. Fink, H. Brauer, A. Fischer, G. Hausdorf, A novel approach to temporary stenting: Degradable cardiovascular stents produced from corrodible metal—Results 6–18 months after implantation into New Zealand white rabbits. *Heart* **86**, 563–569 (2001).
17. M. Peuster, C. Hesse, T. Schloo, C. Fink, P. Beerbaum, C. von Schnakenburg, Long-term biocompatibility of a corrodible peripheral iron stent in the porcine descending aorta. *Biomaterials* **27**, 4955–4962 (2006).
18. D. Zhang, W. Wang, Z. Liu, U.S. Patent US96941115B2 (2017).
19. W. Lin, L. Qin, H. Qi, D. Zhang, G. Zhang, R. Gao, H. Qiu, Y. Xia, P. Cao, X. Wang, W. Zheng, Long-term in vivo corrosion behavior, biocompatibility and bioresorption mechanism of a bioresorbable nitrided iron scaffold. *Acta Biomater.* **54**, 454–468 (2017).
20. W.-J. Lin, D.-Y. Zhang, G. Zhang, H.-T. Sun, H.-P. Qi, L.-P. Chen, Z.-Q. Liu, R.-L. Gao, W. Zheng, Design and characterization of a novel biocorrodible iron-based drug-eluting coronary scaffold. *Mater. Des.* **91**, 72–79 (2016).
21. J.-F. Zheng, H. Qiu, Y. Tian, X.-Y. Hu, T. Luo, C. Wu, Y. Tian, Y. Tang, L.-F. Song, L. Li, L. Xu, B. Xu, R.-L. Gao, Preclinical evaluation of a novel sirolimus-eluting iron bioresorbable coronary scaffold in porcine coronary artery at 6 months. *JACC Cardiovasc. Interv.* **12**, 245–255 (2019).
22. K. Kolandaivelu, R. Swaminathan, W. J. Gibson, V. B. Kolachalama, K. L. Nguyen-Ehrenreich, V. L. Giddings, L. Coleman, G. K. Wong, E. R. Edelman, Stent thrombogenicity early in high-risk interventional settings is driven by stent design and deployment and protected by polymer-drug coatings. *Circulation* **123**, 1400–1409 (2011).
23. S. Bangalore, B. Toklu, N. Patel, F. Feit, G. W. Stone, Newer-generation ultrathin strut drug-eluting stents bersus older second-generation thicker strut drug-eluting stents for coronary artery disease: Meta-analysis of randomized trials. *Circulation* **138**, 2216–2226 (2018).
24. S. Torii, H. Jinnouchi, A. Sakamoto, M. Kutyna, A. Cornelissen, S. Kuntz, L. Guo, H. Mori, E. Harari, K. H. Paek, R. Fernandez, D. Chahal, M. E. Romero, F. D. Kolodgie, A. Gupta, R. Virmani, A. V. Finn, Drug-eluting coronary stents: Insights from preclinical and pathology studies. *Nat. Rev. Cardiol.* **17**, 37–51 (2020).
25. H. Yang, C. Wang, C. Liu, H. Chen, Y. Wu, J. Han, Z. Jia, W. Lin, D. Zhang, W. Li, W. Yuan, H. Guo, H. Li, G. Yang, D. Kong, D. Zhu, K. Takashima, L. Ruan, J. Nie, X. Li, Evolution of the degradation mechanism of pure zinc stent in the one-year study of rabbit abdominal aorta model. *Biomaterials* **145**, 92–105 (2017).
26. W. Yu, J. Qiu, J. Xu, C. Zhuo, F. Simescu, H. Idrissi, Effect of zinc phosphate chemical conversion coating on corrosion behaviour of mild steel in alkaline medium: Protection of rebars in reinforced concrete. *Sci. Technol. Adv. Mater.* **9**, 045009 (2008).
27. R. Naderi, M. M. Attar, Application of the electrochemical noise method to evaluate the effectiveness of modification of zinc phosphate anticorrosion pigment. *Corros. Sci.* **51**, 1671–1674 (2009).
28. A. Adhilakshimi, K. Ravichandran, T. S. N. S. Narayanan, Protecting electrochemical degradation of pure iron using zinc phosphate coating for biodegradable implant applications. *New J. Chem.* **42**, 18458–18468 (2018).
29. C. H. Mathewson, *Zinc: The Science and Technology of the Metal, Its Alloys and Compounds* (Reinhold Publishing Corporation, ed. 1, 1959).
30. R. Waksman, P. Zumstein, M. Pritsch, E. Wittchow, M. Haude, C. Lapointe-Corriveau, G. Leclerc, M. Joner, Second-generation magnesium scaffold Magmaris: Device design and preclinical evaluation in a porcine coronary artery model. *EuroIntervention* **13**, 440–449 (2017).
31. R. S. Schwartz, E. Edelman, R. Virmani, A. Carter, J. F. Granada, G. L. Kaluza, N. A. F. Chronos, K. A. Robinson, R. Waksman, J. Weinberger, G. J. Wilson, R. L. Wilensky, Drug-eluting stents in preclinical studies: Updated consensus recommendations for preclinical evaluation. *Circ. Cardiovasc. Interv.* **1**, 143–153 (2008).
32. LifeTech Brings You a Look Back at the Highlights of CIT 2018 (2018); www.lifetechmed.com/en/news/n1/20180612/2070.aspx.
33. C. Simon, J. C. Palmaz, E. Sprague, Influence of topography on endothelialization of stents: Clues for new designs. *J. Long Term Eff. Med. Implants* **10**, 143–151 (2000).
34. P. Lanzer, G. Strupp, W. Schmidt, L. D. T. Topoleski, The need for stent-lesion matching to optimize outcomes of intracoronary stent implantation. *J. Biomed. Mater. Res. B Appl. Biomater.* **101**, 1560–1570 (2013).
35. Y. Sotomi, Y. Onuma, C. Collet, E. Tenekecioglu, R. Virmani, N. S. Kleiman, P. W. Serruys, Bioresorbable scaffold: The emerging reality and future directions. *Circ. Res.* **120**, 1341–1352 (2017).
36. J. Liu, B. Zheng, P. Wang, X. Wang, B. Zhang, Q. Shi, T. Xi, M. Chen, S. Guan, Enhanced in vitro and in vivo performance of Mg-Zn-Y-Nd alloy achieved with APTES pretreatment for drug-eluting vascular stent application. *ACS Appl. Mater. Interfaces* **8**, 17842–17858 (2016).
37. E. Tenekecioglu, P. W. Serruys, Y. Onuma, R. Costa, D. Chamié, Y. Sotomi, T.-B. Yu, A. Abizaid, H.-B. Liew, T. Santoso, Randomized comparison of absorb bioresorbable vascular scaffold and mirage microfiber sirolimus-eluting scaffold using multimodality imaging. *JACC Cardiovasc. Interv.* **10**, 1115–1130 (2017).
38. S. K. Yazdani, A. Sheehy, M. Nakano, G. Nakazawa, M. Vorpahl, F. Otsuka, R. S. Donn, L. E. Perkins, C. A. Simonton, F. D. Kolodgie, R. Virmani, Preclinical evaluation of second-generation everolimus- and zotarolimus-eluting coronary stents. *J. Invasive Cardiol.* **25**, 383–390 (2013).

Acknowledgments: We thank J. Wang of Yale University (New Haven, USA) and Z. Yang of Southwest Jiaotong University (Chengdu, China) for revising our manuscript and R. Virmani of CVPath Institute (Gaithersburg, USA) for the endothelialization evaluation. **Funding:** This work was supported by the National Key R&D Program of China (grant no. 2018YFC1106600); Shenzhen Industrial and Information Technology Bureau (grant no. 20180309174916657); the Science, Technology and Innovation Commission of Shenzhen Municipality (grant no. GJHZ20180418190517302); and the National Natural Science Foundation of China (grant no. 51931001). **Author contributions:** W.L. and D.Z. conceived the study. H.Q., D.B., W.Z., S.W., and X.S. performed the experiments. H.Q., D.S., and L.Q. analyzed the data. G.Z. performed the animal experiments and the corresponding tests. W.F. performed the mechanical experiments. R.G., K.D., and B.X. performed the clinical studies and collected the samples and clinical data. J.R. performed the FIB and TEM experiments and analyses. M.A. performed the scaffold implantation in the arterial duct of an infant with pulmonary atresia with intact ventricular septum (PAIVS). Y.Z. and D.S. prepared the figures and wrote the manuscript with the help of Z.Y., and R.G. provided oversight. All the authors read and approved the final manuscript. **Competing interests:** Patents: It is declared that D.Z. is the inventor on a patent related to this work filed by Biotyx Medical (Shenzen) Co. Ltd (no. CN104207866B, filed 30 May 2013, published 7 December 2016). D.Z. and W.L. are inventors on a patent related to this work filed by Biotyx Medical (Shenzen) Co. Ltd (no. CN105686897B, filed 28 November 2014, published 19 March 2019). D.Z. is the inventor on a patent related to this work filed by Biotyx Medical (Shenzen) Co. Ltd (no. CN103705324B, filed 31 December 2013, published 29 June 2016). D.Z. is the inventor on a patent related to this work filed by Biotyx Medical (Shenzen) Co. Ltd (no. CN105636618B, filed 31 October 2014, published 28 September 2018). H.Q., W.L., and D.Z. are inventors on a patent related to this work filed by Biotyx Medical (Shenzen) Co. Ltd (no. CN106474545B, filed 8 January 2016, published 10 April 2020). H.Q., W.L., and D.Z. are inventors on a patent related to this work filed by Biotyx Medical (Shenzen) Co. Ltd (no. US10946121B2, filed 27 June 2016, published 16 March 2021). W.L. is the inventor on a patent related to this work filed by Biotyx Medical (Shenzen) Co. Ltd (no. CN106333773B, filed 7 July 2015, published 8 May 2018). Financial relationships: D.Z. is a minority shareholder of Lifetech Scientific (Shenzhen) Co. Ltd. The authors declare that they have no other competing interests. **Data and materials availability:** All data needed to evaluate the conclusions in the paper are present in the paper and/or the Supplementary Materials. Additional data related to this paper may be requested from the authors.

Submitted 8 October 2020
Accepted 19 April 2021
Published 4 June 2021
10.1126/sciadv.abf0614

Citation: D. Shen, H. Qi, W. Lin, W. Zhang, D. Bian, X. Shi, L. Qin, G. Zhang, W. Fu, K. Dou, B. Xu, Z. Yin, J. Rao, M. Alwi, S. Wang, Y. Zheng, D. Zhang, R. Gao, PDLLA-Zn-nitrided Fe bioresorbable scaffold with 53-μm-thick metallic struts and tunable multistage biodegradation function. *Sci. Adv.* **7**, eabf0614 (2021).